nature nanotechnology

SUPPLEMENTARY INFORMATION

https://doi.org/10.1038/s41565-018-0339-0

In the format provided by the authors and unedited.

A piezoelectric, strain-controlled antiferromagnetic memory insensitive to magnetic fields

Han Yan[1,7], Zexin Feng[1,7], Shunli Shang[2], Xiaoning Wang[1], Zexiang Hu[1], Jinhua Wang[3,4], Zengwei Zhu[3,4], Hui Wang[1], Zuhuang Chen[5], Hui Hua[1], Wenkuo Lu[1], Jingmin Wang[1], Peixin Qin[1], Huixin Guo[1], Xiaorong Zhou[1], Zhaoguogang Leng[1], Zikui Liu[2], Chengbao Jiang[1], Michael Coey[1,6] and Zhiqi Liu[1]*

[1]School of Materials Science and Engineering, Beihang University, Beijing, China. [2]Department of Materials Science and Engineering, The Pennsylvania State University, University Park, PA, USA. [3]Wuhan National High Magnetic Field Center, Huazhong University of Science and Technology, Wuhan, China. [4]School of Physics, Huazhong University of Science and Technology, Wuhan, China. [5]School of Materials Science and Engineering, Harbin Institute of Technology, Shenzhen, China. [6]Department of Pure and Applied Physics, Trinity College, Dublin, Ireland. [7]These authors contributed equally: Han Yan, Zexin Feng. *e-mail: zhiqi@buaa.edu.cn

Supplementary Figures

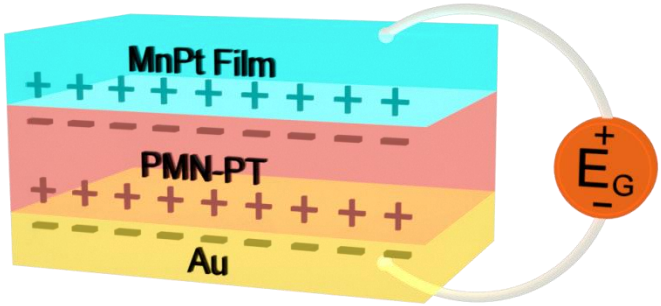

Supplementary Figure 1| Schematic of the electrostatic doping of the MnPt film by a negative gate electric field E_G via the ferroelectric $0.72PbMg_{1/3}Nb_{2/3}O_3$–$0.28PbTiO_3$ (PMN-PT) substrate in a MnPt/PMN-PT heterostructure.

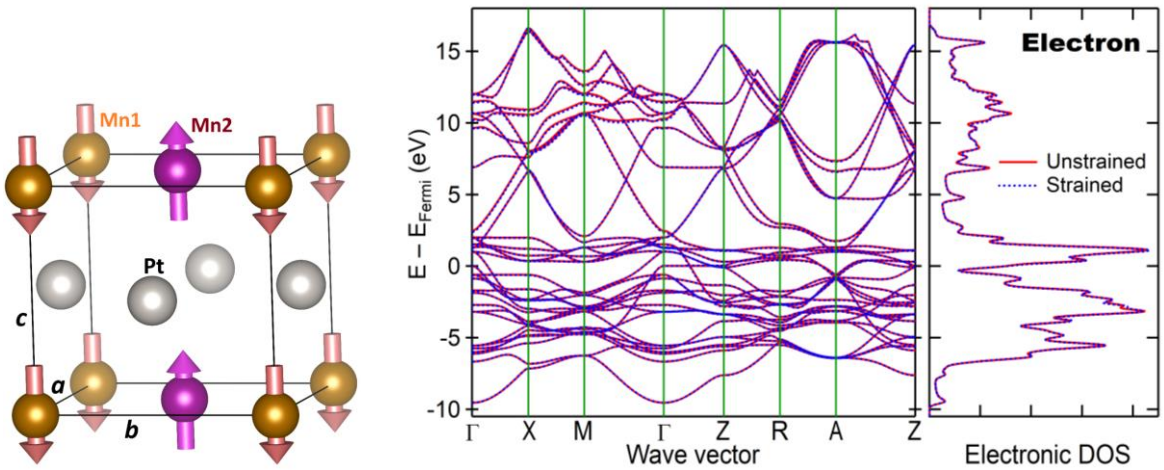

Supplementary Figure 2| Influence of strain on the electronic band structure and density of states (DOS) of antiferromagnetic (AFM) MnPt. Electronic band structure and electronic DOS of AFM MnPt. Note that only the spin up parts are plotted due to the AFM nature of MnPt since the spin down parts are the same as those of the spin up parts. The electronic structures of MnPt are almost unchanged with a small compressive strain of 0.1% along the *a*- and *b*-axis directions.

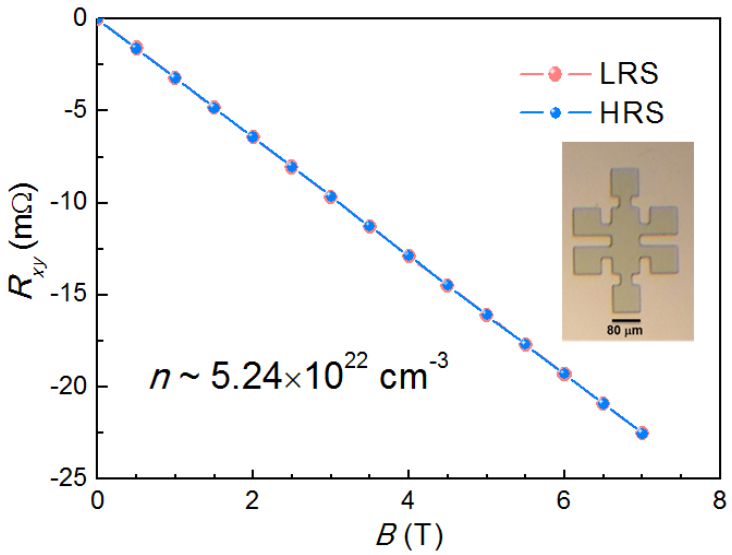

Supplementary Figure 3| Room-temperature Hall effect of the textured MnPt film at different resistance states. Inset: A typical Hall bar pattern for the measurements.

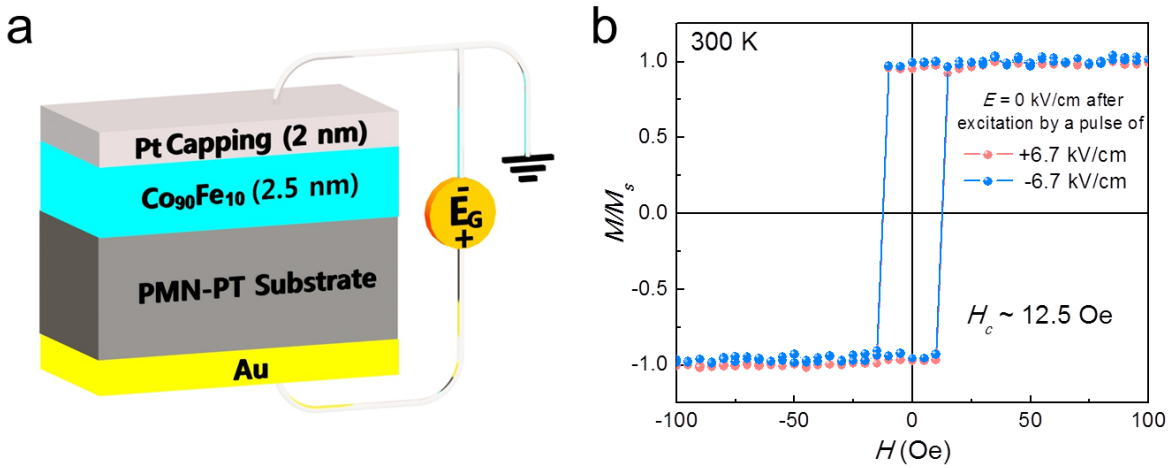

Supplementary Figure 4| Effect of electric pulses on the magnetic properties of a $Co_{90}Fe_{10}$ film. a, Schematic of the electric switch geometry. **b,** Magnetic hysteresis loops of the $Co_{90}Fe_{10}$ film after excitation by positive/negative electric field pulses.

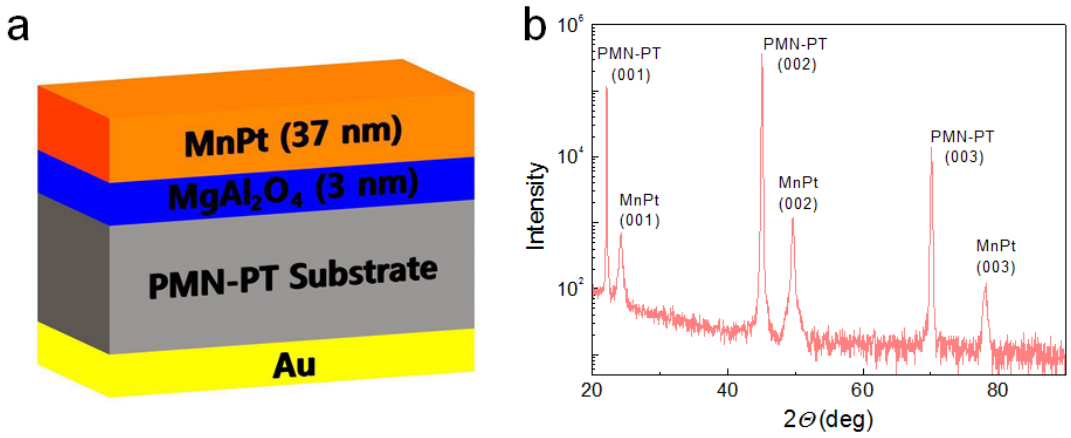

Supplementary Figure 5| Epitaxial MnPt/MAO/PMN-PT heterostructure fabricated by high-temperature growth. a, Schematic of the epitaxial MnPt/MAO/PMN-PT heterostructure. **b,** X-ray diffraction of the heterostructure.

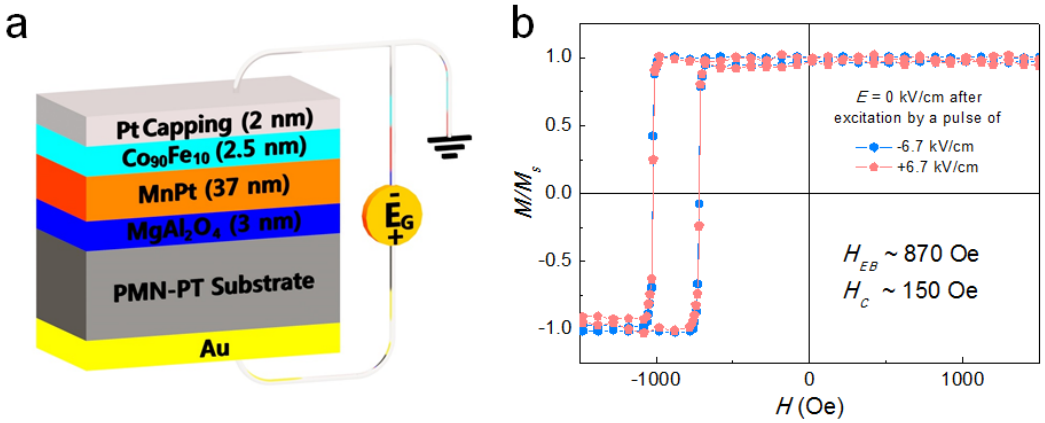

Supplementary Figure 6| Exchange bias in the $Co_{90}Fe_{10}$/epitaxial MnPt system. a, Schematic of the sample structure and electrical connection for applying electric pulses. **b,** Exchange bias after excitations by positive and negative electric field pulses.

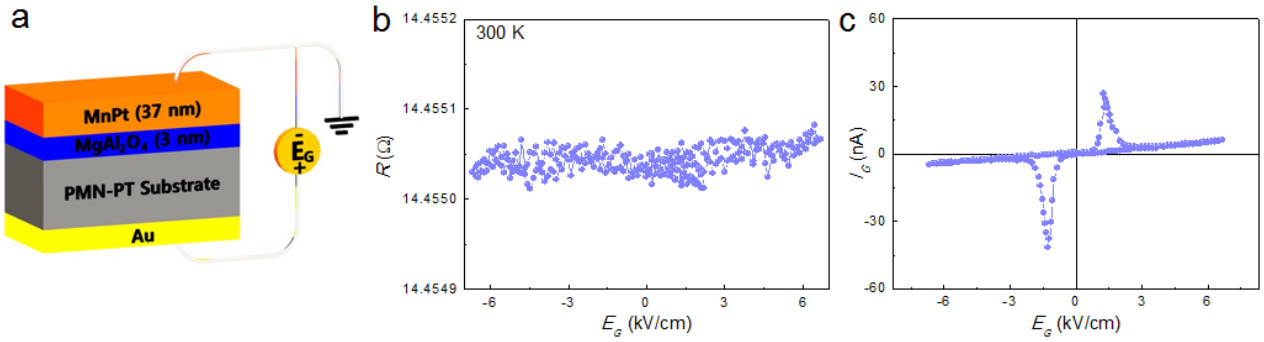

Supplementary Figure 7| Electroresistance of a (001)-ordered MnPt/MAO/PMN-PT heterostructure. a, Schematic of the sample structure and the gate field geometry for electroresistance measurements. **b,** E_G-dependent resistance of the (001)-oriented MnPt single-crystalline film. **c,** Perpendicular gating current as a function of E_G.

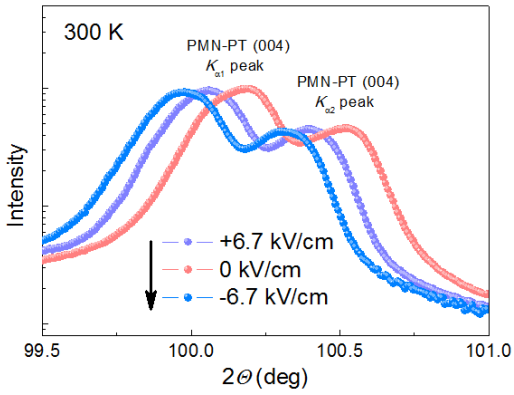

Supplementary Figure 8| Piezoelectric strain. X-ray diffraction of the PMN-PT (004) peak under different electric fields in an epitaxial MnPt/MAO/PMN-PT heterostructure.

Supplementary Notes

Supplementary Note 1: Grain sizes of (001)- and (101)-oriented grains

According to the Scherrer formula, the grain size D can be inferred from $D = 0.89\lambda/(\beta\cos\theta)$, where λ is the X-ray wavelength, β is the peak width at half maximum and θ is the diffraction angle. λ is 1.54056 Å. Based on Fig. 1b, β is 0.647° and 0.690° for the (001) and (101)-oriented grains, respectively. θ is 24.738° and 20.088° for the (002) and (101) peak, respectively. Therefore, the grain size for (001)- and (101)-oriented grains is ~13.4 and ~12.1 nm, respectively.

Supplementary Note 2: Electrostatic doping

As shown in Fig. S1, a negative gate electric field E_G applied from the bottom Au gate induces positive surface charges on the ferroelectric $0.72PbMg_{1/3}Nb_{2/3}O_3$–$0.28PbTiO_3$ (PMN-PT) surface adjacent to the Au electrode and negative surface charges on the top surface, which subsequently induces additional positive carriers (holes) in the MnPt films via the electrostatic induction. As a result, the electrons in the MnPt film are, to some extent, depleted and thus the resistance of the MnPt film increases.

Supplementary Note 3: Density functional theory calculations

The structure of antiferromagnetic (AFM) MnPt is shown on the left in Fig. S2, which is the lowest energy configuration based on our previous examination[1]. All density functional theory

(DFT) based first-principles calculations were performed by the Vienna *Ab* initio Simulation Package[2] with the ion-electron interaction depicted by the projector augmented wave method[3], and the exchange-correlation functional described by the generalized gradient approximation developed by Perdew, Burke, and Ernzerhof[4]. During the Vienna *Ab* initio Simulation Package calculations, 7 electrons ($3d^5 4s^2$) were treated as valence electrons for Mn and 10 ($5d^9 6s^1$) for Pt. The energy convergence criterion for electronic self-consistency was at least 10^{-6} eV per atom and the plane wave cutoff energy of 337 eV was employed. The *k*-points meshes were (18×18×18) for MnPt with 4 atoms in the primitive cell and (6×6×6) for the 32-atom supercell for phonon calculations.

Supplementary Note 4: Control experiments with (001)-oriented MnPt single crystalline films

We performed high-temperature growth to fabricate highly-ordered (001)-oriented MnPt films on PMN-PT substrates by inserting 3-nm-thick $MgAl_2O_4$ buffer layers. PMN-PT is not chemically stable at temperatures higher than 550 °C due to the volatile nature of Pb. A $MgAl_2O_4$ buffer layer could prevent the loss of Pb at its surface and also serves as an epitaxial template for MnPt growth. A $MgAl_2O_4$ layer was first deposited on to a PMN-PT substrate by radio frequency sputtering with 100 W and an Ar pressure of 3 mTorr at 500 °C. After that, a 37 nm MnPt layer was grown at 600 °C and post-annealed in vacuum at 800 °C for 1 h. The X-ray diffraction of a MnPt/ $MgAl_2O_4$/PMN-PT heterostructure is shown in Fig. S5, which indicates that MnPt is fully (001)-oriented.

To confirm the AFM nature of epitaxial MnPt films, 2.5 nm $Co_{90}Fe_{10}$ and 2 nm Pt layers are similarly deposited on top of them. As seen in Fig. S6, such a heterostructure exhibits a large exchange bias field H_{EB} of ~245 Oe and a coercivity field H_c of 150 Oe, which is consistent with our previous work[1]. More importantly, the large exchange bias in the $Co_{90}Fe_{10}$/(001)-ordered MnPt system does not change upon external electric field excitations. Meanwhile, we examined the effect of electric fields/strain on the resistivity of fully (001)-oriented MnPt. As shown in Fig. S7, although the polarization switching in PMN-PT can be clearly seen in the E_G-dependent perpendicular current curve (Fig. S7c), the electroresistance effect is negligible. This also helps rule out the electron-phonon scattering mechanism as the dominant origin for the electroresistance. Overall, these results support our assumption that strain rotates the AFM spin

axis of (101)-oriented grains in textured MnPt films, leading to enhanced exchange coupling with $Co_{90}Fe_{10}$ and also the low-resistance state.

In addition, the piezoelectric strain generated from PMN-PT with a 3 nm $MgAl_2O_4$ buffer layer on top, *i.e.*, in the MnPt/ $MgAl_2O_4$/PMN-PT/Au structure was found to be similar to that in the MnPt/PMN-PT/Au structure (Fig. S8).

Supplementary References:

1. Liu, Z. *et al.* Epitaxial growth of intermetallic MnPt films on oxides and large exchange bias. *Adv. Mater.* **28**, 118–123 (2016).

2. Kresse, G. & Furthmüller, J. Efficient iterative schemes for *Ab initio* total-energy calculations using a plane-wave basis set. *Phys. Rev. B* **54**, 11169–11186 (1996).

3. Kresse, G. & Joubert, D. From ultrasoft pseudopotentials to the projector augmented-wave method. *Phys. Rev. B* **59**, 1758–1775 (1999).

4. Perdew, J. P., Burke, K. & Ernzerhof, M. Generalized gradient approximation made simple. *Phys. Rev. Lett.* 77, 3865–3868 (1996).